⌘ *Author's Choice*

THE JOURNAL OF BIOLOGICAL CHEMISTRY VOL. 283, NO. 46, pp. 31679–31689, November 14, 2008

Iron-mediated Aggregation and a Localized Structural Change Characterize Ferritin from a Mutant Light Chain Polypeptide That Causes Neurodegeneration*

Received for publication, July 21, 2008, and in revised form, August 26, 2008 Published, JBC Papers in Press, August 28, 2008, DOI 10.1074/jbc.M805532200

Martin A. Baraibar[‡], Ana G. Barbeito[‡], Barry B. Muhoberac[§], and Ruben Vidal[‡1]

From the [‡]Department of Pathology and Laboratory Medicine, Indiana University School of Medicine and the [§]Department of Chemistry and Chemical Biology, Indiana University-Purdue University Indianapolis, Indianapolis, Indiana 46202

Nucleotide insertions in the ferritin light chain (FTL) polypeptide gene cause hereditary ferritinopathy, a neurodegenerative disease characterized by abnormal accumulation of ferritin and iron in the central nervous system. Here we describe for the first time the protein structure and iron storage function of the FTL mutant *p.Phe167SerfsX26* (MT-FTL), which has a C terminus altered in sequence and extended in length. MT-FTL polypeptides assembled spontaneously into soluble, spherical 24-mers that were ultrastructurally indistinguishable from those of the wild type. Far-UV CD showed a decrease in α-helical content, and 8-anilino-1-naphthalenesulfonate fluorescence revealed the appearance of hydrophobic binding sites. Near-UV CD and proteolysis studies suggested little or no structural alteration outside of the C-terminal region. In contrast to wild type, MT-FTL homopolymers precipitated at much lower iron loading, had a diminished capacity to incorporate iron, and were less thermostable. However, precipitation was significantly reversed by addition of iron chelators both *in vitro* and *in vivo*. Our results reveal substantial protein conformational changes localized at the 4-fold pore of MT-FTL homopolymers and imply that the C terminus of the MT-FTL polypeptide plays an important role in ferritin solubility, stability, and iron management. We propose that the protrusion of some portion of the C terminus above the spherical shell allows it to cross-link with other mutant polypeptides through iron bridging, leading to enhanced mutant precipitation by iron. Our data suggest that hereditary ferritinopathy pathogenesis is likely to result from a combination of reduction in iron storage function and enhanced toxicity associated with iron-induced ferritin aggregates.

Iron is an essential element needed for vital processes such as neuronal development, myelination, synthesis, and catabolism of neurotransmitters and electron transport, as well as heme and iron-sulfur cluster synthesis (1). Iron that is not utilized immediately in the cell is stored in ferritin. However, when iron is improperly regulated, it is potentially toxic leading to cell death. Mammalian ferritin is a large, iron-storage heteropolymer composed of two conformationally equivalent subunit types, light (FTL)[2] and heavy (FTH1) polypeptides, which are expressed in most kinds of cells (2–5). A single ferritin protein is composed of 24 self-assembled polypeptide subunits related by 4-, 3-, and 2-fold symmetry axes with one polypeptide per asymmetric unit. Each polypeptide subunit consists of a bundle of four parallel α-helices (A–D), a long extended loop (connecting helices B and C), and a C terminus with a short α-helix (E), which is involved in important stabilizing interactions around the 4-fold symmetry axes (2, 6, 7). Although both types of polypeptide subunits share a high degree of conformational similarity, they have diverse functional roles. The FTH1 subunit has a potent ferroxidase activity that catalyzes the oxidation of ferrous iron, whereas the FTL subunit plays important roles in iron nucleation and protein stability, giving ferritin the dual functions of iron detoxification and iron storage (2). Interestingly, the FTL homopolymer has iron incorporation ability, although at a substantially reduced rate from heteropolymers containing both FTL and FTH1 subunits (2).

Recently, nucleotide insertions in the coding sequence of the *FTL* gene (8–11) have been found associated with an autosomal dominant neurodegenerative disease named neuroferritinopathy (8) or hereditary ferritinopathy (HF) (9). Clinically, HF is characterized by an abnormal involuntary movement disorder and cognitive decline, which may appear sequentially between the 3rd and 6th decades of life. Neuropathologically, the disease is characterized by the presence of intracellular ferritin inclusion bodies and iron accumulation in glia and neurons throughout the central nervous system and other organ systems (12). Three different mutations have been found in individuals with neuropathologically confirmed HF, an adenosine insertion at position 460–461 (8), a thymidine and cytidine insertion at position 498–499, (9), and a cytidine insertion at position 442–443 (10). As a consequence of these mutations, the FTL polypeptides have C termini that are each changed in length and primary amino acid sequence. Two additional mutations in the *FTL* gene, a point mutation at codon 96 (13) and a 16 nucle-

* This work was supported, in whole or in part, by National Institutes of Health Grant NS050227 (to R. V.). The costs of publication of this article were defrayed in part by the payment of page charges. This article must therefore be hereby marked "*advertisement*" in accordance with 18 U.S.C. Section 1734 solely to indicate this fact.

⌘ *Author's Choice*—Final version full access.

[1] To whom correspondence should be addressed: Dept. of Pathology and Laboratory Medicine, Indiana University School of Medicine, 635 Barnhill Dr., MSB A136, Indianapolis, IN 46202. Tel.: 317-274-1729; Fax: 317-278-6613; E-mail: rvidal@iupui.edu.

[2] The abbreviations used are: FTL, ferritin light chain; WT-FTL, wild type ferritin light chain; MT-FTL, mutant (*p.Phe167SerfsX26*) ferritin light chain; FTH1, ferritin heavy chain; ANS, 8-anilino-1-naphthalenesulfonate; TEM, transmission electron microscopy; GdnHCl, guanidine hydrochloride; FAC, ferric ammonium citrate; Phen, 1, 10-phenanthroline; DFX, deferroxamine; IREs, iron-responsive elements; HF, hereditary ferritinopathy; GFAP, glial fibrillary acidic protein; PBS, phosphate-buffered saline.

otide insertion (11), have been described in clinically diagnosed individuals.

Here we characterize the protein structure and the iron storage function of ferritin formed by the polypeptide *p.Phe167SerfsX26*, generated by the *FTL498–499InsTC* mutation (MT-FTL) (9). The mutant polypeptide assembled spontaneously into ferritin spherical shells in a soluble manner. Spectroscopic and proteolytic analysis of these mutant ferritin homopolymers showed a large protein conformational difference with the wild type FTL (WT-FTL) homopolymers in the C terminus. Compared with WT-FTL homopolymers, those of the MT-FTL were less stable, had a diminished capacity to incorporate iron, and precipitated at iron:ferritin ratios of over 1,000 iron atoms per ferritin 24-mer. However, precipitation was greatly reversed by the addition of iron chelators both *in vitro* and *in vivo*. The results shown here suggest that the C terminus of the MT-FTL polypeptide plays an important role not only in the solubility and stability of ferritin, but also in iron management, and provide insights into the molecular mechanisms involved in the generation of ferritin inclusion bodies and the accumulation of iron observed in patients with HF.

EXPERIMENTAL PROCEDURES

Cloning and Expression of Ferritin Polypeptides—cDNAs containing the sequence of human WT-FTL and human mutant *FTL498–499InsTC* were introduced into the pET-28a(+) expression vector (Novagen, EMD Chemicals Inc.). The cDNAs were cloned between the BamHI and XhoI sites, downstream from and in-frame with the sequence encoding an N-terminal His_6 tag. To eliminate the His_6 tag (included in the expression vector), the sequence of the vector was modified by introducing the recognition sequence for cleavage by factor Xa before the coding sequence of the ferritin genes. PCR amplification of the ferritin cDNAs was performed using the upstream primer F1 5′-TGG ATC CAT CGA AGG TCG TAT GAG CTC CCA GAT T-3′ and the downstream primer R1 5′-TTA TGC CTC GAG CCC TAT TAC TTT GCA AGG-3′. F1 contains the factor Xa sequence (underlined). pET-28a(+) carrying WT-FTL and MT-FTL cDNAs was transformed into BL21 (DE3) *Escherichia coli* (Invitrogen). Transformed cells were grown in Luria broth medium (LB) containing 30 μg/ml kanamycin (Invitrogen) at 37 °C up to an absorbance of 0.9–1.0 at 600 nm. Bacteria were induced to overexpress recombinant proteins by adding 1 mM isopropyl thio-β-D-galactopyranoside (ICN Biotechnologies) for 12 h at 25 °C.

Purification of Recombinant WT- and MT-FTL Homopolymers—Cells were harvested by centrifugation and frozen at −80 °C. The cell pellets were suspended in 50 mM sodium phosphate, 500 mM NaCl (pH 7.4), 1 mg/ml lysozyme, and a protease inhibitor mixture (Complete, Roche Applied Science) for 30 min. Bacteria were disrupted by sonication, and the insoluble material was removed by centrifugation at 21,000 × *g* for 30 min. The soluble fraction was purified by nickel iminodiacetic acid affinity chromatography using an AKTA purifier system (GE Healthcare). Purified protein was eluted with 250 mM imidazole in 50 mM sodium phosphate (pH 7.4), 0.5 M NaCl. Recombinant proteins were diluted with 50 mM Tris and 10% glycerol (v/v) down to an absorbance of 0.5 at 280 nm, and ferritins were cleaved from the His tag by digestion with factor Xa protease (GE Healthcare) (5 units/mg of protein). After being dialyzed against 50 mM Tris, pH 8.0, for 18 h, proteins were further purified by anion exchange chromatography (Mono Q) using a linear NaCl elution gradient in 50 mM Tris (pH 8). Peak fractions were ~95% pure based on SDS-12% PAGE (Pierce) and Coomassie Blue staining. The efficiency of tag removal was confirmed by N-terminal protein sequencing analysis, and the molecular weight of the recombinant proteins was determined by matrix-assisted laser desorption/ionization-time of flight mass spectrometry. Protein concentration was determined using the BCA reagent (Pierce) with bovine serum albumin as standard.

Gel Filtration Chromatography—Size exclusion chromatography was performed on a Superose 6 10/300 GL column (GE Healthcare) equilibrated with 50 mM Tris, 150 mM NaCl (pH 7.4) using an AKTA purifier. The column was calibrated with gel filtration standards (GE Healthcare). Fractions were detected photometrically, and peak areas and k_{av} values were evaluated using the UNICORN 5.1 software (GE Healthcare). All gel filtration experiments were run at room temperature.

Transmission Electron Microscopy (TEM)—Ferritins were fixed using the "single droplet" parafilm protocol. The specimens were dropped onto a 400-mesh carbon/Formvar-coated grid (Nanoprobes) and allowed to absorb to the Formvar for a minimum of 1 min. Excess fluid was removed using filter paper, and the unbound protein was washed, and the grids were placed on a 50-μl drop of Nanovan (Nanoprobes) with the section side downwards. Finally, the grids were dried, placed in the grid chamber, and stored in desiccators before the samples were observed with a Tecnai G2 12 Bio Twin (FEI) transmission electron microscope.

Preparation of Apoferritins—Recombinant FTL homopolymers were treated for iron removal as described previously (14). Briefly, recombinant ferritins were incubated with 1% thioglycolic acid (pH 5.5) and 2,2′-bipyridine, followed by dialysis against 0.1 M phosphate buffer (pH 7.4). We consistently achieve less than five atoms of iron per ferritin 24-mer, as determined by the colorimetric ferrozine-based assay for the quantitation of iron (15).

Iron Loading of Apoferritins—Freshly prepared ferrous ammonium sulfate (0.5–4.5 mM) in 10 mM HCl was added to MT- and WT-FTL apoferritin homopolymers (1 μM) in 0.1 M Hepes buffer (pH 7.4) at room temperature (16). After 2 h, the samples were centrifuged at 14,000 × *g* for 15 min. Iron incorporation was initially monitored by measuring absorbance of the supernatants at 310 nm (14, 17). Iron incorporation into ferritin was more precisely determined by densitometric analysis of Prussian blue staining of supernatants run on nondenaturing gel electrophoresis. Pellets were analyzed by SDS-12% PAGE. Apoferritins were also incubated in a molar ratio 1:3500 with ferrous ammonium sulfate and centrifuged at 14,000 × *g* for 15 min. Pellets were resuspended in a solution containing 6 mM deferroxamine (DFX), 0.1 M Hepes (pH 7.4) and incubated for 2 h at 24 °C. After centrifugation, supernatants were analyzed by nondenaturing gel electrophoresis.

Circular Dichroism Spectroscopy—CD spectra of recombinant apoferritin homopolymers were obtained in 50 mM phos-

phate buffer (pH 7.4) at 25 °C in a Jasco 810 spectropolarimeter (Jasco Corp.), using a protein concentration of 0.12 and 1.5 μM for far-UV and near-UV, respectively. Far-UV CD spectra were recorded in a 1.0-mm path length cell from 250 to 190 nm with a step size of 0.1 nm and a bandwidth of 1.0 nm. Each spectrum represents the mean of 15 scans. CD spectra of the buffer/cuvette were recorded and subtracted from the protein spectra before averaging. Secondary structure analyses were performed using DICHROWEB (18, 19), which allows secondary structure analyses via the software package CDPro (20). SELCON3 (21), CONTINLL (22), and CDSSTR (23) programs were used for comparing variations in the amount of secondary structure between MT- and WT-FTL homopolymers. Normalized root mean square deviation values of < 0.1 for the three methods meant that the experimental and simulated spectra were in close agreement. Near-UV CD spectra were recorded in a 1.0-cm path length cell from 400 to 250 nm with a step size of 1.0 nm and a bandwidth of 1.5 nm. For all spectra, an average of five scans was obtained.

Intrinsic Protein Fluorescence and Thermal Stability Studies of Homopolymers—Fluorescence spectra were recorded using a spectrofluorimeter (PerkinElmer Life Sciences) equipped with a Selecta Ultraterm water bath for temperature control. Apoferritin spectra were obtained with excitation at 280 and 295 nm with 1.5 μM protein in 1-cm path length cells and with 0.1 M phosphate (pH 7.4). Blanks without protein were subtracted from the spectra. Thermal denaturation was induced by increasing the temperature from 20 to 100 °C at a rate of 1 °C/min. To overcome the inherent difficulty in denaturing ferritin, these experiments were performed in 0.1 M phosphate buffer (pH 7.4) containing 4.0 M guanidine hydrochloride (GdnHCl). Homopolymer stability was monitored using the ratio of intrinsic fluorescence emission of 355 over 330 nm with excitation at 295 nm (24, 25) with a maximum at 330 nm signifying native ferritin (mt and WT) and 355 nm, denatured ferritin.

ANS Fluorescence and Binding Studies—Extrinsic fluorescence spectra were recorded using a spectrofluorimeter (PerkinElmer Life Sciences) in 1.0-cm cuvettes at 25 °C. ANS binding to apoferritin homopolymers was monitored through fluorescence enhancement with ANS excitation at 360 nm and emission recorded from 600 to 400 nm. MT-FTL apoferritins were prepared by diluting stock solutions to 1.5 μM in 0.05 M phosphate buffer (pH 7.4). Stock solutions of ANS (Invitrogen) were prepared in water, and the concentration was determined optically at 350 nm using an extinction coefficient of 4950 M^{-1} cm^{-1}. ANS was added to the diluted ferritin samples and equilibrated for 30 min prior to the measurements, and spectra were background corrected. Binding of ANS to ferritin was quantitated by Scatchard analysis (26).

Thermolysin Treatment of WT- and MT-FTL Apoferritin Homopolymers—Proteolysis of recombinant MT- and WT-FTL homopolymers was initiated by adding to 10 μg of ferritin a 10-fold concentrated stock solution (36.5 units/mg) of thermolysin (Fluka) in Hepes (0.1 M) (pH 7.0), 10 mM $CaCl_2$ to a final concentration of 0.2 mg/ml. The reaction was stopped by the addition of EDTA (50 mM) and Laemmli sample buffer. Samples treated with thermolysin and controls without thermolysin were boiled and loaded onto SDS-polyacrylamide gels (4–20%) (Pierce). Gels were stained with Coomassie Blue (Total protein) or blotted against the C-terminal antibodies (MT-1283 or WT-1278) (9) or against the N-terminal antibody D18 (Santa Cruz Biotechnology, Inc), which recognized both polypeptides.

Astrocyte Cell Cultures and Iron/Chelator Treatment—Primary cortical astrocyte cultures were prepared from 1-day-old mouse pups according to the procedures of Saneto and De Vellis (27) and Cassina *et al.* (28), with minor modifications. Pups were obtained from transgenic dams homozygous for the *FTL498–499InsTC* mutation in C57BL/6J genetic background (29). Briefly, cerebral cortices were removed, and the tissue was minced and dissociated in 0.25% trypsin (Invitrogen) for 15 min at 37 °C. Cells were collected by centrifugation and plated at a density of 2.0×10^6 cells in 25-cm^2 flasks (Corning Glass) in Dulbecco's modified Eagle's medium supplemented with 10% fetal bovine serum, Hepes (25 mM), penicillin (100 IU/ml), and streptomycin (100 μg/ml) (Invitrogen). When confluent, cultures were shaken for 48 h at 250 rpm at 37 °C, incubated for another 48 h with 10 μM cytosine arabinoside, and then amplified to 2.5×10^4 cells/cm^2 in 75-cm^2 flasks (Corning Glass). The astrocyte monolayers were >98% pure as determined by GFAP immunoreactivity. Confluent astrocyte monolayers were changed to Dulbecco's modified Eagle's media devoid of serum prior to treatment. Stock solutions (20 mM) of ferric ammonium citrate (FAC) (Sigma), and 1,10-phenanthroline (Phen) (Sigma) were prepared in distilled water and directly applied to the monolayer at the indicated final concentrations. Each flask was treated with either of the following: (*a*) vehicle (water) as control group; (*b*) Phen at 100 μM during 48 h followed by 24 h at 50 μM; (*c*) FAC 50 μM during 4 days; (*d*) FAC treatment as in *c* followed by Phen treatment as in *b* in the absence of iron.

Characterization of Detergent-insoluble MT-FTL Ferritin from Astrocyte Cultures—Cerebral cortical astrocytes cultures were homogenized in lysis buffer (3 ml of 50 mM Tris-HCl (pH 7.4), 1% SDS, 30 units/ml benzonase, 2 mM $MgCl_2$) containing Complete protease inhibitor mixture (Roche Applied Science) and incubated for 15 min at room temperature. Lysates containing equal amounts of protein were ultracentrifuged at 46,000 rpm (TLA 110, Beckman) for 25 min at 4 °C. The supernatant (SDS-soluble) was removed, and the SDS-insoluble pellet was resuspended in lysis buffer and then subjected to another step of centrifugation in the same conditions. The final pellet was resuspended in 5× Laemmli sample buffer and heated for 10 min at 95 °C. The SDS-soluble, -insoluble, and total cell lysates (before SDS extraction) were resolved on 4–20% gradient SDS-PAGE (Pierce) and transferred to nitrocellulose membranes (Amersham Biosciences). Membranes were blocked for1 h in 70 mM Tris-buffered saline, 0.1% Tween 20, and 5% nonfat dry milk, followed by an overnight incubation with polyclonal antibodies (1283) against the MT-FTL polypeptide, as described previously (9, 29) at 1:10,000. After washing, membranes were incubated with peroxidase-conjugated secondary antibody (GE Healthcare) for 1 h, washed, and developed using the ECL chemiluminescent detection system (GE Healthcare). MT-FTL recombinant polypeptides were loaded and used as positive control.

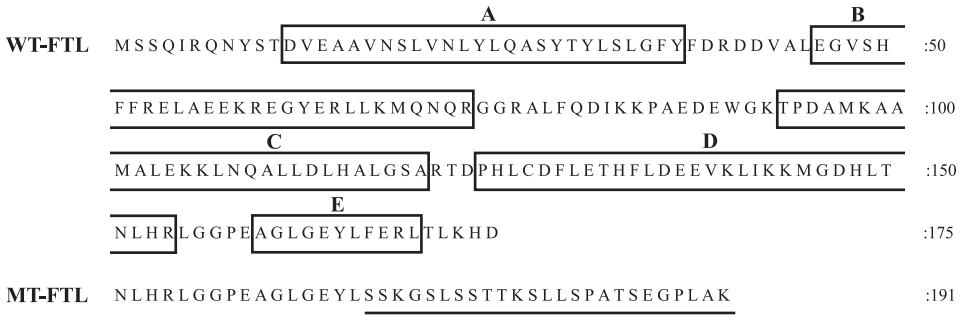

FIGURE 1. **Sequence comparison between WT- and MT-FTL polypeptide.** The wild type FTL polypeptide (WT-FTL) consists of 175 amino acids. The *p.Phe167SerfsX26* mutant polypeptide (MT-FTL) has 191 amino acids and a different C-terminal sequence (*underlined*). The *boxes* indicate the five α-helical domains in the WT-FTL polypeptide according to Protein Data Bank accession number 2FG4. The mutant C-terminal sequence contains both metal-binding and hydrophobic groups.

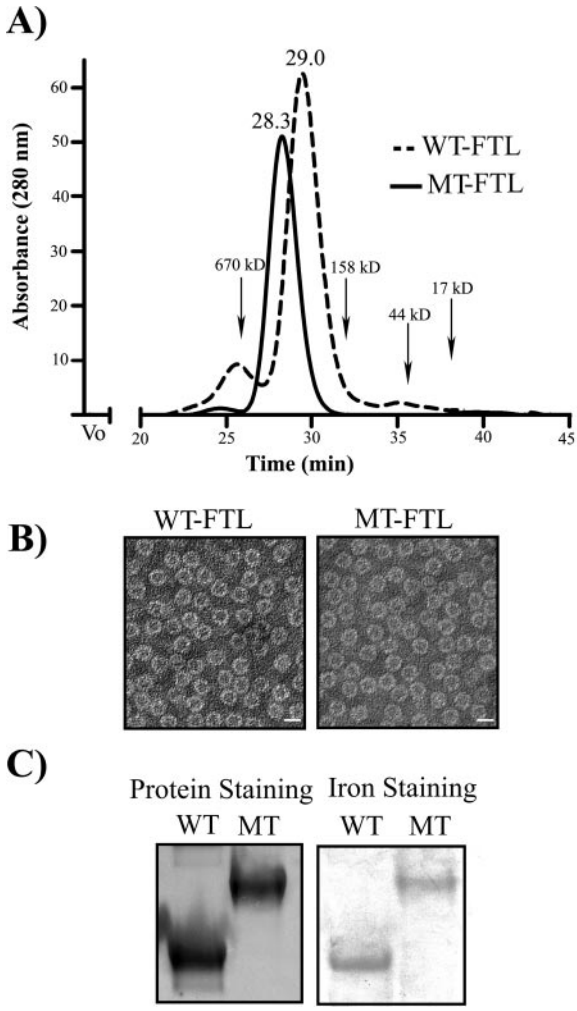

FIGURE 2. **MT-FTL polypeptides assemble into 24-mer homopolymers.** *A,* elution profiles of purified WT- and MT-FTL apoferritin homopolymers from a Superose 6 column at pH 7.4 in 0.05 M Tris, 0.15 M NaCl. Retention times for both proteins are shown. *Arrows* indicate the elution time for the molecular weight markers. *B,* ultrastructural characterization of WT- and MT-FTL homopolymers by TEM. The dark cores most likely represent Nanovan that has penetrated in some cases the interior of the 24-mers. *Bars,* 10 nm. *C,* native PAGE (3–8% (pH 7.4)) of 0.5 μM WT- and MT-FTL proteins loaded before the removal of iron and stained with Coomassie Blue (protein staining) and with Prussian blue (iron staining).

Immunofluorescence of Cultured Cells—Astrocyte cultures in Lab-Tek chambered coverglass slides (Nunc) were fixed for 15 min with 4% paraformaldehyde in PBS at 4 °C. Briefly, the slides were washed successively with PBS, permeabilized with 0.1% Triton X-100 for 15 min, and incubated for 1 h at room temperature in blocking solution (0.1% Triton X-100, 2% bovine serum albumin in PBS). The cultures were incubated overnight at 4 °C with the primary antibodies diluted in blocking solution, washed with PBS, and further incubated for 1 h at room temperature with the secondary antibodies diluted in blocking solution. The slides were then washed with PBS, rinsed with distilled water, and mounted with the Prolong Gold antifade mounting reagent (Molecular Probes). Primary antibodies used were monoclonal antibody to GFAP (1:400; Sigma) and polyclonal antibody against MT-FTL (1283). Secondary antibodies used were Alexa 488 Fluor-conjugated goat anti-rabbit and Alexa Fluor 594-conjugated goat anti-mouse (4 μg/ml; Molecular Probes). Images were captured with a Zeiss LSM-510 confocal scanner attached to a Zeiss Axiovert 100 M inverted microscope.

RESULTS

Recombinant MT-FTL Polypeptides Assemble into 24-mer Homopolymers—Recombinant WT- and MT-FTL polypeptides (Fig. 1) were expressed in *E. coli* in a soluble manner and with similar yields. Purified WT- and MT-FTL polypeptides were analyzed by gel filtration chromatography to determine their states of assembly at physiological pH. Both polypeptides eluted almost exclusively as 24-mer homopolymers, but at slightly different times (Fig. 2*A*) in a manner consistent with their difference in molecular mass. Ultrastructural analysis by TEM showed that both recombinant ferritins had spherical shape and a size (diameter ~110 Å) similar to that of human ferritin (Fig. 2*B*). Nondenaturing PAGE showed that both WT- and MT-FTL homopolymers, examined before iron removal, were able to assemble and incorporate iron *in vivo* during expression in *E. coli* (Fig. 2*C*). Compared with WT-FTL homopolymers, MT-FTL homopolymers showed a slower electrophoretic mobility, which may be attributed to their larger size and different charge (the MT-FTL polypeptide has a +1 net charge difference per subunit) (Fig. 2*C*).

Enhanced Precipitation of MT-FTL Homopolymers—Iron loading of apoferritin homopolymers was examined by an often used and well described procedure (14, 16, 17). In brief, WT- and MT-FTL apoferritin homopolymers were incubated aerobically with increasing amounts of iron (ferrous ammonium sulfate) up to 4500 iron atoms per 24-mer. After 2 h, proteins were separated by centrifugation into soluble and insoluble (pellet) fractions for analysis. Monitoring the 310 nm absorbance (Fig. 3*A*) suggested that at moderate iron loading (up to 1,000 iron atoms per ferritin 24-mer), the WT- and MT-apoferritin homopolymers incorporated similar amounts of iron indicating that both are functional ferritins. At higher iron:fer-

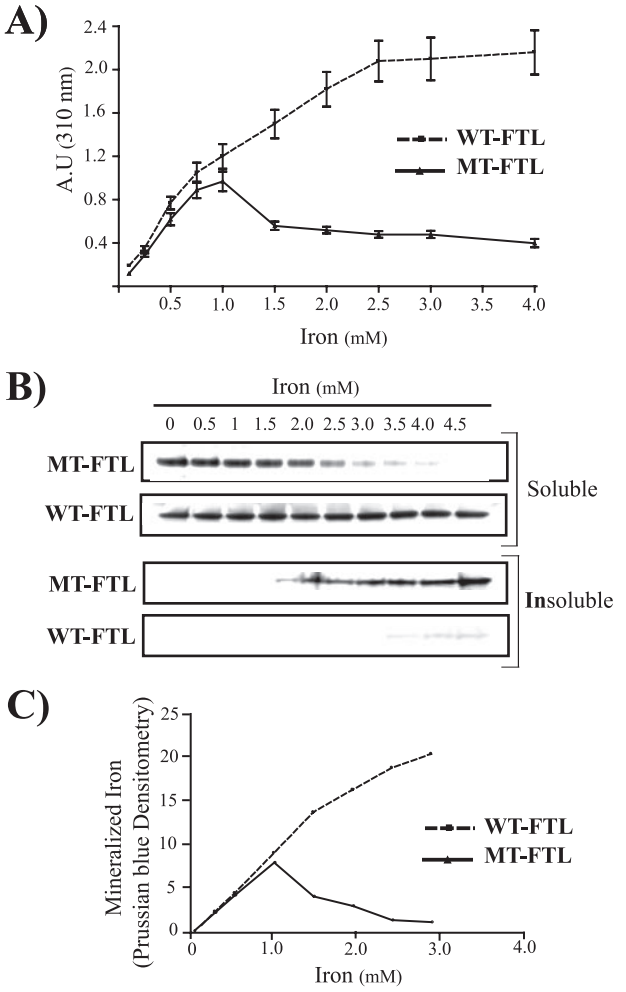

FIGURE 3. **Precipitation of MT-FTL apoferritin homopolymers mediated by iron loading.** Ferrous ammonium sulfate (0.5–4.5 mM) was added to 1 μM of MT- and WT-FTL homopolymers in 0.1 M Hepes (pH 7.0) for 2 h at 24 °C. Samples were centrifuged for 15 min at 10,000 × *g* to separate into soluble and insoluble fractions. *A,* iron uptake/hydrolysis was monitored in the soluble fractions by measuring absorbance at 310 nm. *Errors bars* represent the standard deviation of three independent experiments. *B,* soluble and insoluble fractions were loaded into native gels SDS-PAGE, respectively, and stained with Coomassie Blue. *C,* iron mineralization in soluble MT- and WT-FTL homopolymers was monitored as the density of Prussian blue formed in protein bands after separating unmineralized iron from the protein by electrophoresis in native gels (3–8%). This experiment is representative of several with similar results.

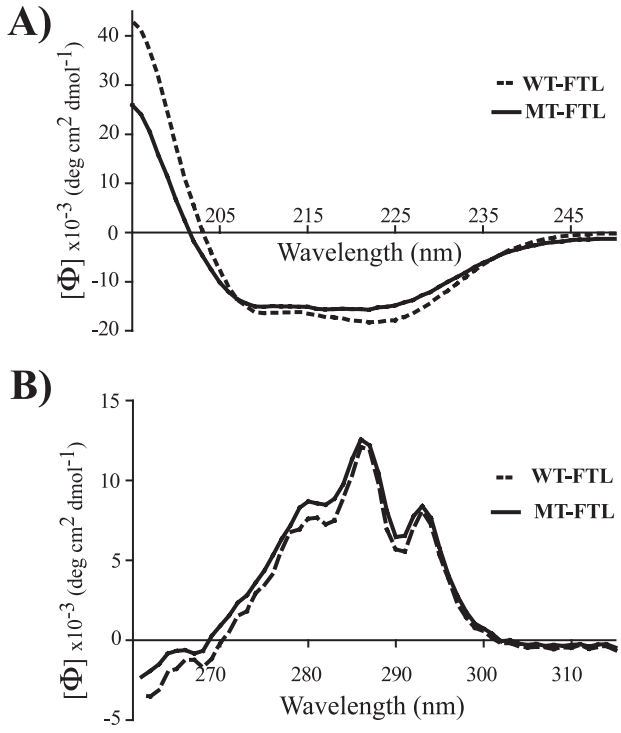

FIGURE 4. **Circular dichroism spectra of WT- and MT-FTL apoferritin homopolymers.** Far-UV (*A*) and near-UV (*B*) spectra were recorded at homopolymer concentrations of 0.12 and 1.5 μM, respectively, at pH 7.4 and 25 °C in 50 mM potassium phosphate buffer.

ritin ratios, WT-FTL homopolymers continued incorporating iron, whereas MT-FTL homopolymers began to show macroscopically visible yellow precipitates, which were stained with Prussian blue. No precipitates were observed for WT-FTL homopolymers, which remained in the soluble fraction during the iron loading experiment up to a ratio of 4500:1 of iron: ferritin. The reduction in the signal observed in native PAGE for soluble MT-FTL homopolymers correlated with the appearance of MT-FTL in the insoluble fraction on SDS-PAGE (Fig. 3*B*). Because the 310 nm absorbance represents both iron incorporation and hydrolysis, the soluble ferritin fractions (supernatants) were run on nondenaturing gels and stained with Prussian blue to unambiguously quantitate iron incorporation into the protein. There was only a modest (~10%) decrease in iron incorporation in MT-FTL homopolymers *versus* wild type at 1000:1 iron:ferritin loading (Fig. 3*C*), which emphasizes iron mishandling through mutant ferritin precipitation. By TEM, MT-FTL precipitates had the shape of apoferritin homopolymers (data not shown).

Spectroscopic Comparison of MT-FTL Apoprotein Homopolymers Versus WT—Protein spectra provide molecular level information concerning protein structure and especially structural differences between similarly composed proteins. The far-UV CD spectrum of MT-FTL apoferritin showed minima at 222 and 208 nm and a maximum at 191–193 nm (Fig. 4*A*). The profile obtained was typical of a protein containing predominantly α-helical motifs. Compared with the WT-FTL homopolymers, we observed a change in the secondary structure of MT-FTL, with a decrease of ~15% in the total α-helical content and an increase in turns and unordered structures (Table 1). Near-UV CD was performed to provide a "fingerprint" profile of MT-FTL apoferritin. The profile obtained for MT-FTL homopolymers was very similar to that obtained for the WT-FTL, with the WT predominant peak at 286 nm and two other peaks at 293 and 280 nm (Fig. 4*B*). The intrinsic fluorescence spectra exhibited an emission maximum at approximately the same wavelength (330 nm) for both WT- and MT-ferritins when both proteins were excited at either 280 or 295 nm (data not shown).

ANS Binding to MT-FTL Homopolymers—ANS fluorescence intensity enhancement occurs upon its binding to hydrophobic sites on proteins. ANS binding assays were performed to study the occurrence of exposed hydrophobic surfaces in MT-FTL apoprotein homopolymers. In aqueous medium, ANS shows an emission maximum at 515 nm, but when this reagent binds to a hydrophobic moiety, its fluorescence intensity increases sever-

alfold, and the emission maximum is blue-shifted to 470 nm. At pH 7.4, native ferritin does not bind ANS nor does it fully denatured ferritin (24, 30). However, a large increase in ANS fluorescence at 470 nm was observed when ANS was added to the MT-FTL homopolymers, indicating exposed hydrophobic sites (Fig. 5*A*). A saturation curve exhibiting noncooperative binding was observed following titration of ANS into MT-FTL homopolymers (Fig. 5*B*). Scatchard analyses resulted in a linear plot with an apparent dissociation constant in the micromolar range.

Decreased Thermal Stability of MT- Versus WT-FTL Apoferritin Homopolymers—The thermal stability of the apoferritin homopolymers was monitored by measuring the change in intrinsic fluorescence of the protein as the structure is perturbed. The unusual stability of ferritins necessitated the addition of a perturbing agent to partially destabilize the protein making it accessible to denaturation by heating (31, 32). Using established procedures (24, 25) the protein was excited at 295 nm in the presence of 4.0 M GndHCl, and the extent of denaturation was quantitated as a ratio of emission intensities. With increasing temperature, the fluorescence emission maxima shifted from 330 nm (native) to 355 nm (denatured) for both WT- and MT-FTL homopolymers (Fig. 6*A*). Both transitions were two-state, and transition midpoint temperatures (T_m) were calculated from the curves (Fig. 6*B*). WT-FTL homopolymers had the highest T_m (~90 °C), which decreased markedly with MT-FTL (~45 °C). Without addition of denaturant, MT-FTL exhibited a T_m near 75 °C.

Differential Proteolysis of WT- Versus MT-FTL Homopolymers—In general, limited proteolysis does not usually occur with α-helices, but largely at loops and disordered protein sequences (33, 34). To investigate the possibility of exposed disordered motifs in MT-FTL homopolymers, we conducted limited proteolysis using thermolysin, which displays broad substrate specificity (35). Thermolysin selectively cleaved the mutant and generated a predominant fragment of ~17 kDa. The fragment showed immunoreactivity with an antibody that recognizes the protein N terminus, suggesting that the mutant homopolymer is cleaved at the C terminus. In contrast WT-FTL homopolymers were resistant to thermolysin proteolytic digestion when reacted under identical experimental conditions (Fig. 7).

Chelation of Iron Reverses Iron-induced Aggregation in Vitro—Precipitation of MT-FTL homopolymers was observed when they were loaded with iron (ferrous ammonium sulfate) at greater than 1,000 iron atoms per ferritin 24-mer, whereas WT-FTL homopolymers remained in the soluble fraction at least until loading with 4,500 iron atoms. However, the precipitation of MT-FTL homopolymers was found to be reversible. More specifically, greater than 50% of mutant homopolymers that were precipitated by treatment with 3500:1 iron:ferritin was resolubilized by incubation with the chelator DFX (Fig. 8).

Chelation of Iron Reverses Iron-induced Aggregation in Vivo—To investigate iron-mediated aggregation *in vivo*, we used primary cultures of astrocytes from cerebral cortex of transgenic mice expressing the MT-FTL polypeptide. In this mouse model, the human MT-FTL polypeptide forms heteropolymers with the endogenous murine wild type Ftl and Fth1 polypeptides, which are seen to aggregate in neurons and glia throughout the life span of the mice (29). After treatment of the cells with FAC to increase their intracellular iron stores, we observed a switch of ferritin from the detergent-soluble fraction to the detergent-insoluble fraction, suggesting a change in the solubility (Fig. 9*A*). Addition of the lipophilic and freely cell-permeant iron chelator 1,10-Phen to the FAC-treated cells (FAC/Phen) led to a large reduction in the signal for detergent-insoluble ferritin and the reappearance of ferritin in the detergent-soluble fraction (Fig. 9*A*). For these *in vivo* experiments, Phen was preferred over the weakly cell-permeant DFX that was used for the *in vitro* experiments. Addition of Phen alone did not seem to have a significant effect on the amount of ferritin present in the detergent-insoluble or -soluble fractions isolated from the cultured astrocytes. Double immunolabeling experiments showed intranuclear accumulation of ferritin as well as the presence of small, punctate ferritin deposits in the cellular cytoplasm (Fig. 9, *CT*). Importantly, addition of FAC to astrocytes expressing MT-FTL led

TABLE 1

Deconvolution of far-UV CD spectra for wt- and mt-FTL apoferritin homopolymers into percent secondary structural contributions

The analysis was performed using fitting programs ContnnLL, SELCON3, and CDSSTR available at the website DICHROWEB as described under "Experimental Procedures."

	α-Helix[a]	β-Sheet[a]	Turns	Other
MT-FTL				
ContinnLL	0.55	0	0.1	0.36
SELCON3	0.58	0	0.1	0.32
CDSSTR	0.57	0	0.1	0.34
WT-FTL				
ContinnLL	0.72	0	0	0.28
SELCON3	0.69	0	0.1	0.3
CDSSTR	0.72	0	0	0.28

[a] Regular fraction is indicated.

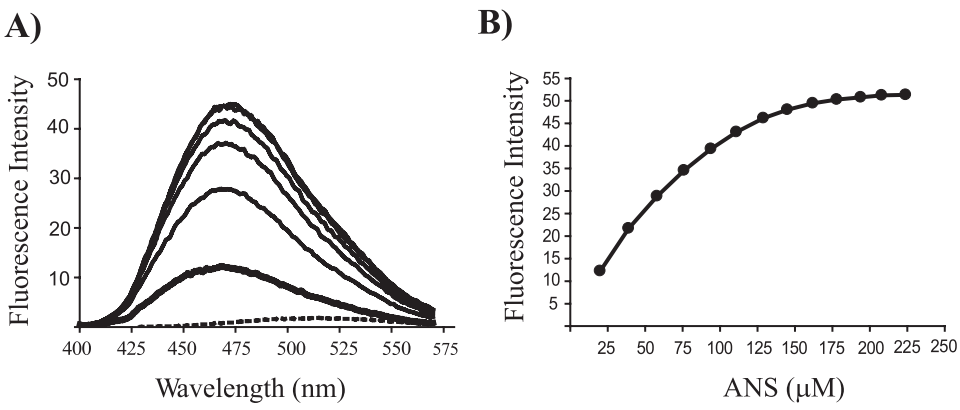

FIGURE 5. **Binding of ANS to MT-FTL apoferritin homopolymers.** *A,* ANS fluorescence emission enhancement and wavelength shift caused by titration of MT-FTL homopolymers with increasing concentrations of ANS. *B,* background and dilution corrected fluorescence emission intensity at 460 nm as a function of ANS concentration. Titration was performed on 1.5 μM MT-FTL homopolymer at pH 7.4 and 25 °C in 50 mM potassium phosphate buffer. The *dotted line* corresponds to 100 μM ANS in potassium phosphate buffer.

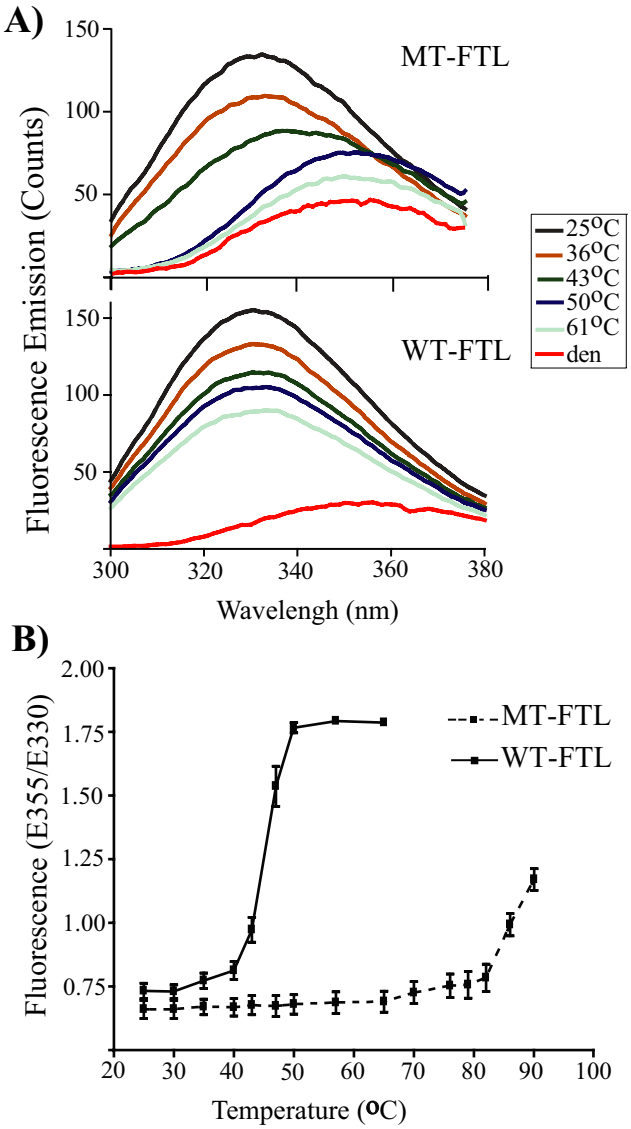

FIGURE 6. **Decrease in thermal stability of MT- *versus* WT-FTL apoferritin homopolymers.** *A,* temperature dependence of fluorescence emission spectra of MT- and WT-FTL homopolymers destabilized by 4.0 M GdnHCl. The *red trace* represents denatured ferritin (*den*) induced by incubation at pH 2.0 in 4.5 M GdnHCl. *B,* fluorescence emission intensity ratio (of 355 over 330 nm) to determine denaturation temperature of both apoferritin homopolymers. Scans were performed on 1.5 μM ferritin homopolymer at pH 7.4 in potassium phosphate buffer with excitation at 295 nm. Homopolymers were incubated 12 h in 4.5 M GdnHCl before beginning temperature dependence experiment. *Errors bars* represent the standard deviation of three independent experiments.

to an increase in the signal for MT-FTL (Fig. 9*B*, *FAC*), which correlated with an increase in the amount of detergent-insoluble ferritin observed by Western blot analysis. We also observed that FAC treatment led to astrocyte reactivity, characterized by a redistribution of the intermediate filament GFAP and the formation of long cytoplasmic processes (Fig. 9*B*, *FAC*) as described previously (28). Addition of Phen after incubation with FAC partially reversed the astrocytic reactive phenotype and decreased the cellular immunolabeling for ferritin (Fig. 9*B*, *FAC/Phen*). No significant differences with the control were observed when only the chelator was added to the cell culture (Fig. 9, *Phen*).

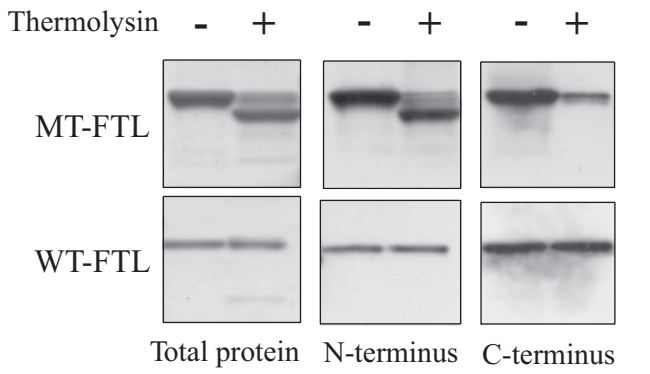

FIGURE 7. **Thermolysin treatment of WT- and MT-FTL apoferritin homopolymers.** Recombinant MT- and WT-FTL homopolymers (1 μM) were incubated with thermolysin (0.15 units) in Hepes buffer (0.1 M) (pH 7.0), 60 mM NaCl, 1 mM $CaCl_2$. After 10 min at 37 °C, the reaction was quenched with 10 μl of EDTA (50 mM). Sample buffer was added, and the samples treated with thermolysin (+), and controls without thermolysin (−) were loaded onto 4–20% SDS-PAGE. Gels were stained with Coomassie Blue (*Total protein*) or blotted using antibodies specific for the N terminus of FTL or the C terminus of MT-FTL or WT-FTL.

DISCUSSION

In this work we investigate the protein structure and iron storage function of ferritin homopolymers formed from a light chain variant *p.Phe167SerfsX26* that causes HF (9). Both wild type FTH1 and FTL polypeptide subunits are important for the iron storage function of ferritin, with the former containing the ferroxidase site for ferrous iron oxidation and the latter containing the iron nucleation site (2, 3). However, homopolymers composed of FTL subunits have additional properties such as resistance to precipitation under iron loading and being significantly more stable to denaturation by heat and solvent (30, 36), and apparently FTL subunits are able to confer these properties upon the heteropolymer. Thus as the first approach to elucidating the effects of the mutation, we compared and contrasted wild type with MT-FTL homopolymers, which have a C terminus of altered length and composition (9).

Gel filtration and nondenaturing electrophoretic analyses showed that at physiological pH, recombinant MT-FTL polypeptides were able to assemble as 24-mer homopolymers, which were ultrastructurally indistinguishable from homopolymers of recombinant WT-FTL polypeptide. However, homopolymers made of the mutant subunit showed a smaller retention time and a slower electrophoretic mobility compared with those of the WT-FTL polypeptide, consistent with the molecular mass difference. Homopolymers of recombinant WT- and MT-FTL polypeptides were able to incorporate iron *in vivo* in preparations obtained from *E. coli*, suggesting that both are functional proteins. *In vitro*, recombinant WT- and MT-apoferritin homopolymers incorporated similar amounts of iron up to 1000:1 iron:ferritin molar ratio over a 2-h incubation. However, at higher iron:ferritin ratios, WT-FTL homopolymers continued incorporating iron, whereas MT-FTL homopolymers began to precipitate, limiting their iron storage function.

To understand this functional difference, MT- and WT-FTL apoferritins were analyzed by spectroscopic techniques. Such techniques are particularly useful in revealing differences

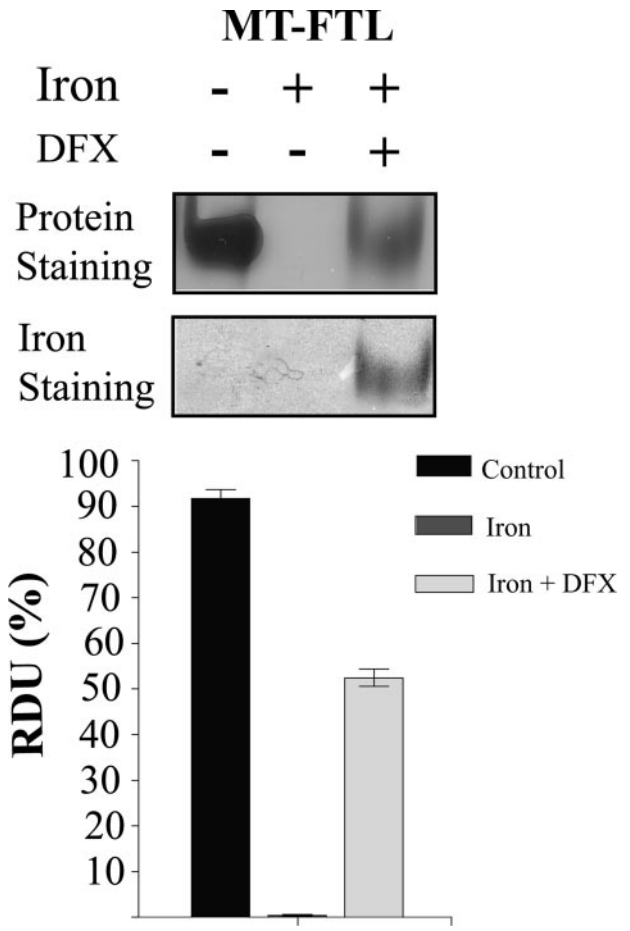

FIGURE 8. **Iron-induced aggregation of MT-FTL homopolymers and its reversal by the iron chelator deferroxamine.** MT-FTL homopolymers were incubated in a molar ratio 1:3500 with ferrous ammonium sulfate as in Fig. 3. After centrifugation, the pellet was resuspended in a solution containing 6 mM DFX, 0.1 M Hepes (pH 7.4) and incubated for 2 h at 24 °C. After a second centrifugation, soluble fractions were run in native gels and stained with Coomassie Blue for protein and with Prussian blue for iron. Densitometric analysis of the protein bands was performed, and the values are shown as relative densitometric units (*RDU*) as a percentage of the control without iron for each protein. All data are expressed as the mean ± S.D. of three independent experiments. WT-FTL homopolymers did not precipitate after iron treatment (not shown).

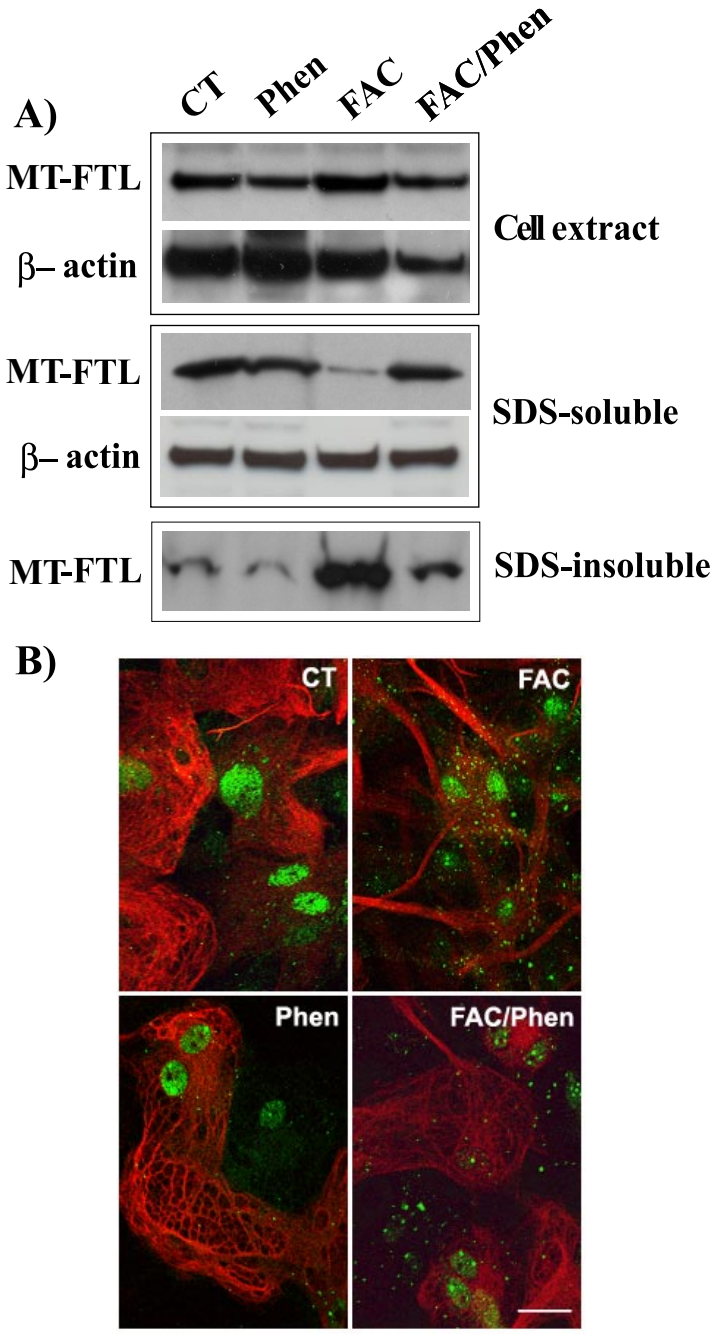

FIGURE 9. **Iron-induced aggregation of cellular ferritin and its reversal by the chelator phenanthroline.** *A,* immunoblot for MT-FTL ferritin from total cell extracts and their SDS-insoluble and SDS-soluble fractions. Transgenic astrocytes were exposed to water (*CT*); 50 μM ferric ammonium citrate for 72 h (*FAC*); 50 μM phenanthroline for 72 h (*Phen*); or 50 μM ferric ammonium citrate for 72 h following 72 h of the iron chelator phenanthroline (50 μM) (*FAC/Phen*). To verify similar loading, membranes were reprobed with anti-actin antibodies. *B,* confocal immunofluorescence microscopy of cultured MT-FTL-transgenic astrocytes treated as in *A*. Cells were immunostained with anti MT-FTL antibody (*green*) and anti-GFAP antibody (*red*). Note the increase in MT-FTL signal after iron treatment (FAC). The signal was greatly decreased after treatment with the chelator (FAC/Phen). *Bar,* 20 μm.

between similarly structured proteins. In the far-UV, the CD spectra of the MT-FTL homopolymers showed a decrease (~15%) in total α-helical content and an increase in turns and unordered structures compared with the WT-FTL. Such a 15% decrease could be accounted for precisely by complete unraveling of the shortest α-helical segment of ferritin (the E helix, located at the C terminus) or alternatively some fraction of portions of the longer helical segments A–D. The E helix involvement is supported by the length and position of the mutation itself (9, 12). The CD data are in agreement with secondary structural prediction analysis (Jpred) (37) and analysis for α-helical context (ProtScale) (38), both of which are consistent with a loss of the E helical domain in the MT-FTL polypeptide.

The CD spectra of the MT- and WT-FTL homopolymers in the near-UV region, which reflects the packing environment of the tyrosines and tryptophans, were very similar. This similarity suggests that the mutation in the FTL polypeptide introduces only a minor change in tertiary and/or quaternary structures of ferritin, which is in agreement with the ability to form the assembled state observed by gel filtration chromatography and nondenaturing PAGE. The minor spectral difference at 280 nm is likely produced by structural perturbation around tyrosine.

One out of the six tyrosines in FTL is located in its C-terminal sequence (amino acid 165) and is present in the WT- and MT-FTL polypeptides. No additional tyrosines or tryptophans are introduced by the mutation to contribute spectral intensity at 280–300 nm. Routine scans of the endogenous protein fluorescence with excitation at 280 and 295 nm gave no difference between WT- and MT-FTL homopolymers (data not shown). However, a structural difference between WT- and MT-FTL homopolymers was revealed by titration with the exogenous fluorophore ANS, which increases its fluorescence and shifts its emission maximum upon interaction with a nonpolar environment. ANS fluorescence was enhanced in a manner indicating equilibrium binding to a hydrophobic pocket that is formed in the mutant. Taken together, the spectroscopic studies are consistent with no changes in the helix content and packing of the 4-helix bundle (A–D) or in the majority of the intersubunit interactions, but with an unraveling of the E helix in the mutant such as to create hydrophobic binding sites for ANS.

A feature of ferritin 24-mers in general is their high stability to heat and to urea or guanidinium chloride exposure (2). We found that in the presence of 4.5 M GdnHCl, WT-FTL homopolymers denatured with the higher T_m ~90 °C and MT-FTL at ~45 °C. Without addition of the destabilizing agent, MT-FTL denatured near 75 °C, which is reduced considerably from that reported in the literature (30, 32) for the wild type, and again points toward significant destabilization of the mutant. For comparison, FTH1 homopolymers are less stable to heat denaturation than FTL homopolymers, perhaps because of residues located at the intersubunit contacts along the 3- and 4-fold channels and by salt bridges within the 4-helix bundles themselves between Lys-62 and Glu-107 (24, 32). Indeed, native E helix conformation appears to help stabilize the subunit structure of the FTL homopolymer by making several hydrophobic contacts with apolar side chains near the start of helix B and the end of D as well as being linked by hydrogen bonds to the N-terminal ends of helices B and C (2, 6, 7, 39). Given the spectroscopic results, the difference in thermal stability observed between the WT and mutant homopolymers can be attributed to the loss of the interactions around the E helix in the MT-FTL subunit. Although the E helices are known to contribute to the exceptional thermostability of ferritin, they are not essential in the pattern of ferritin assembly (40).

The data presented so far suggest that ferritin accommodates the extensive sequence alteration present in the *p.Phe167SerfsX26* mutant without disturbing its assembly/folding pathway or spherical shell structure. Susceptibility to thermal denaturation was enhanced by the mutation, but not in the physiological range of temperature where it may be directly causative of precipitation. In WT-FTL, the helical C terminus is not accessible, being accommodated inside the spherical surface (as part of the shell structure) and forming the 4-fold pore. However, the disposition of the unraveled C terminus in the mutant was not clearly delineated by spectroscopy or denaturation studies in that it may be contained within the interior, be totally exterior to the shell, or have some intermediate conformation. To investigate the difference in C-terminal conformation between WT and mutant homopolymers, both were subjected to thermolysin proteolysis and the products analyzed by gel electrophoresis and Western blot. The results showed that the C terminus of the MT-FTL homopolymer, but not the WT, was susceptible to proteolysis with ~75% of the sample exhibiting loss. The N terminus was, however, not susceptible to cleavage nor were there other proteolysis products evident. These results strongly support a conformation in which at least part of the C terminus sequence of the mutant extends into the solvent far enough above the well formed, spherical exterior surface to be approached and cleaved by thermolysin for a large fraction of ferritin subunits. Alternatively, a distribution between completely external and completely internal C termini could occur. Thus, not only is the 4-fold pore disrupted, but ferritin has an amino acid sequence protruding external to the shell to interact with its surroundings (including iron). The lack of multiple thermolysin cleavage bands also attests to the intact nature of the mutant homopolymer, paralleling the wild type intactness.

Changes in the C terminus in different ferritin polypeptides exhibit a variety of documented effects. C-terminal deletion of a comparable sequence in the FTH1 polypeptide caused the protein to form oligomers that were unable to incorporate and keep iron in solution (14, 40), whereas lengthening of the FTH1 polypeptide by addition of various amino acid sequences did not modify ferritin assembly. Interestingly, when large peptide sequences were added, they were found to be exposed outside the ferritin shell (14, 40, 42–44). Insertional mutations of a mouse *Fth1* cDNA using nucleotide sequences similar to those associated with HF produced mutant polypeptides of different lengths. In these experiments, the mutant polypeptides showed a significant alteration in protein folding, assembly, and function, which was correlated with the loss of the last helical domain that existed in the WT protein (45). Studies using recombinant mutant FTL (*p.Arg154LysfsX26*), corresponding to the 460–461InsA variant (8) suggested that the recombinant polypeptide was able to assemble into ferritin shells with low efficiency and that the C terminus was exposed outside the shell (46). Analysis of FTL polypeptides with the *p.Phe167SerfsX26* mutation suggest that this mutation is apparently not severe enough to prevent iron incorporation, but it has a C terminus exposed external to the protein shell similar to that associated with the *FTL460–461InsA* mutation and the extended Fth1 polypeptides. Although ferritin formed from our MT-FTL polypeptide precipitated at iron concentration significantly below that of wild type, such precipitation was at least partially reversible. Approximately 50% of ferritin precipitated at a loading of 3500:1 iron:ferritin ratio was resolubilized using the iron chelator DFX, and that resolubilized protein contained iron. Iron-induced aggregation was also seen *in vivo*, but was substantially reversed by the iron chelator Phen. These results argue against large scale structural disruption of the ferritin shells and are in agreement with the spectroscopic and TEM data, which showed that the precipitates had the spherical shape of ferritin.

Significant mutant C-terminal sequence exposure external to a well formed ferritin shell, differential iron-induced precipitation between the mutant and wild type, and reversibility of aggregation by chelation of iron lead to the model of iron-induced aggregation shown in Fig. 10. Specifically, iron can bind

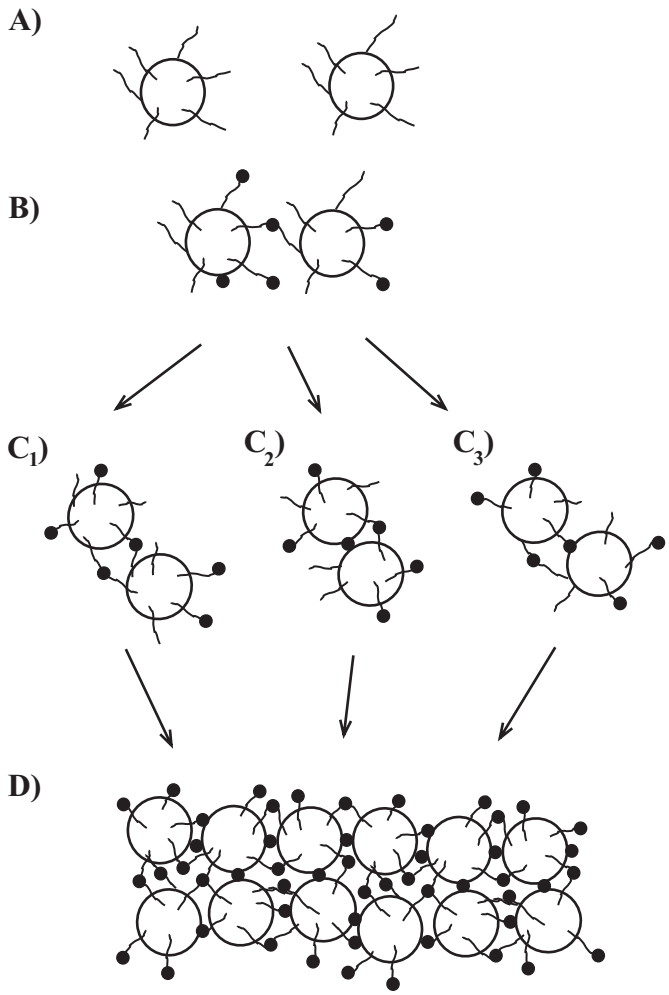

FIGURE 10. **Simplified model describing the steps in the iron-induced aggregation process of mutant ferritin.** *A,* C termini of MT-FTL polypeptides extend above the spherical surface of ferritin exposing this sequence of the peptide to solvent and iron. *B,* sequence binds iron (or iron nucleation complexes) and through it the C terminus of a second MT-FTL polypeptide, reducing the translational motion of both 24-mers. *C,* additional cross-linking occurs (through iron bridges) between C termini, a C terminus and surface carboxylate, and/or eventually through carboxylates on both 24-mers forming ferritin dimers. *D,* dimers aggregate further.

in widely varying affinities to several groups on the exposed C terminus of MT-FTL ferritin. The C-terminal carboxylate, the glutamates, the tyrosinate, and perhaps even the serine hydroxyl, threonine hydroxyl, and peptide backbone groups all can bind iron. The precipitation process appears to begin when an iron (or iron nucleation complexes) binds to groups on the exposed C-terminal regions of two mutant 24-mers preventing their translational motion. Additional C-terminal iron bridging (from other mutant subunits) and/or surface carboxylate (glutamate and aspartate) bridging may occur as the two ferritin shells come together tightening their interaction producing dimers. There is independent evidence of the existence of ferritin dimers in the literature (16, 47), which would agree with involvement of iron-bound carboxylate enhancing bridging. Furthermore, calorimetry studies provide evidence of a large number of weakly bound irons independent of those more tightly bound at the ferroxidase center (41). The process then reaches out to more homopolymers producing precipitation. This process is greatly affected by the redox state of the iron, not just with respect to hydrolysis and formation of precipitated hydroxide complexes, which are part of the bridging and matrix of the ferritin aggregate, but also because the binding strengths of the various groups mentioned above are strongly redox-dependent with ferric iron preferring to bind to hard ligands and ferrous iron generally considered a weaker binder. Finally, the C terminus of the mutant ferritin has hydrophobic patches, which may augment the strength of the bridging interaction and perhaps hinder reversibility by iron chelation. It should be noted that this model is not limited to mutant homopolymers in that heteropolymers with a fraction of MT-FTL polypeptide subunits are not precluded from undergoing iron-induced aggregation. The details of the aggregation process are currently under investigation.

We observed that ferritin precipitates obtained *in vitro* were composed of fully assembled 24-mers, similar to what has been reported in inclusions in patients with HF (9, 12) and in transgenic mice expressing the MT-FTL polypeptide (29). At iron: ferritin ratios above 2000:1, under the same experimental conditions in which we analyzed WT- and MT-FTL, the majority of FTH1 but not WT-FTL ferritins precipitate (16). The precipitation of FTH1 has been suggested to be related to extra-cavity iron hydrolysis (16). Iron-induced aggregation of FTH1 (16) and MT-FTL homopolymers was not irreversible because pellets could be resolubilized by the addition of iron chelators. *In vivo*, we found that the addition of iron led to intracellular accumulation of ferritin in astrocytes from transgenic mice expressing the MT-FTL polypeptide (29). Detergent-insoluble ferritin is typically seen in brain extracts from patients with HF and transgenic mice expressing the MT-FTL polypeptide (29). After iron addition, astrocytic ferritin was found mostly in the detergent-insoluble fraction, indicating that iron-induced ferritin aggregation occurs *in vivo* and may be the mechanism underlying ferritin aggregation in patients with HF. The quantity of detergent-insoluble ferritin was significantly reduced by the addition of the iron chelator Phen to the astrocyte culture, in agreement with the *in vitro* studies.

Our data show that the *FTL498–499InsTC* mutation leads to the generation of FTL polypeptides that are able to assemble into ferritin 24-mers. However, MT-FTL homopolymers have a diminished ability to sequester iron and aggregate well before wild type homopolymers as iron levels are increased. *In vivo*, the MT-FTL polypeptide may act as a dominant negative mutant, leading to a failure of ferritin in its iron storage function and an increase in the levels of intracellular iron. Intracellular free iron generates a positive feedback loop, in which it promotes the release of the iron regulatory proteins from the ferritin iron-responsive elements (2), overexpression of ferritin polypeptides, and the aggregation of mutant-containing ferritins as observed in patients with HF (12) and in transgenic mice (29). Thus we propose that deregulation of cellular iron metabolism and formation of ferritin aggregates, which may physically interfere with normal cellular functions (causing a gain of a toxic function), may be the key pathological mechanisms eventually leading to HF. It should be mentioned that this aggregation mechanism does not exclude other levels of iron mismanagement operating more subtly in addition to it, *e.g.*

iron-induced oxidative stress. Considering the numerous hydrophobic amino acids in the mutant C terminus, a peptide-based iron chelator containing one or more hydrophobic groups may more effectively hinder ferritin aggregation than a simple chelator alone.

Acknowledgments—We are thankful to Dr. B. Ghetti for supportive comments. We gratefully acknowledge the Harvard Microchemistry and Proteomics Analysis Facility for the mass spectrometry and protein sequencing analysis of recombinant proteins and the Indiana Center for Biological Microscopy at Indiana University School of Medicine for the confocal microscopy analysis.

REFERENCES

1. Beard, J. L., and Connor, J. R. (2003) *Annu. Rev. Nutr.* **23,** 41–58
2. Harrison, P. M., and Arosio, P. (1996) *Biochim. Biophys. Acta* **1275,** 161–203
3. Theil, E. C., Matzapetakis, M., and Liu, X. (2006) *J. Biol. Inorg. Chem.* **11,** 803–810
4. Theil, E. C. (2003) *J. Nutr.* **133,** S1549–S1553
5. Liu, X., and Theil, E. C. (2005) *Acc. Chem. Res.* **38,** 167–175
6. Hempstead, P. D., Yewdall, S. J., Fernie, A. R., Lawson, D. M., Artymiuk, P. J., Rice, D. W., Ford, G. C., and Harrison, P. M. (1997) *J. Mol. Biol.* **268,** 424–448
7. Wang, Z., Li, C., Ellenburg, M., Soistman, E., Ruble, J., Wright, B., Ho, J. X., and Carter, D. C. (2006) *Acta Crystallogr. Sect. D Biol. Crystallogr.* **62,** 800–806
8. Curtis, A. R., Fey, C., Morris, C. M., Bindoff, L. A., Ince, P. G., Chinnery, P. F., Coulthard, A., Jackson, M. J., Jackson, A. P., McHale, D. P., Hay, D., Barker, W. A., Markham, A. F., Bates, D., Curtis, A., and Burn, J. (2001) *Nat. Genet.* **28,** 350–354
9. Vidal, R., Ghetti, B., Takao, M., Brefel-Courbon, C., Uro-Coste, E., Glazier, B. S., Siani, V., Benson, M. D., Calvas, P., Miravalle, L., Rascol, O., and Delisle, M. B. (2004) *J. Neuropathol. Exp. Neurol.* **63,** 363–380
10. Mancuso, M., Davidzon, G., Kurlan, R. M., Tawil, R., Bonilla, E., Di Mauro, S., and Powers, J. M. (2005) *J. Neuropathol. Exp. Neurol.* **64,** 280–294
11. Ohta, E., Nagasaka, T., Shindo, K., Toma, S., Nagasaka, K., Ohta, K., and Shiozawa, Z. (2008) *Neurology* **70,** 1493–1494
12. Vidal, R., Delisle, M. B., and Ghetti, B. (2004) *J. Neuropathol. Exp. Neurol.* **63,** 787–800
13. Maciel, P., Cruz, V. T., Constante, M., Iniesta, I., Costa, M. C., Gallati, S., Sousa, N., Sequeiros, J., Coutinho, P., and Santos, M. M. (2005) *Neurology* **65,** 603–605
14. Levi, S., Luzzago, A., Cesareni, G., Cozzi, A., Franceschinelli, F., Albertini, A., and Arosio, P. (1988) *J. Biol. Chem.* **263,** 18086–18092
15. Fish, W. W. (1988) *Methods Enzymol.* **158,** 357–364
16. Levi, S., Santambrogio, P., Cozzi, A., Rovida, E., Corsi, B., Tamborini, E., Spada, S., Albertini, A., and Arosio, P. (1994) *J. Mol. Biol.* **238,** 649–654
17. Levi, S., Salfeld, J., Franceschinelli, F., Cozzi, A., Dorner, M. H., and Arosio, P. (1989) *Biochemistry* **28,** 5179–5184
18. Whitmore, L., and Wallace, B. A. (2004) *Nucleic Acids Res.* **32,** W668–W673
19. Lobley, A., Whitmore, L., and Wallace, B. A. (2002) *Bioinformatics* (*Oxf.*) **18,** 211–212
20. Sreerema, N., and Woody, R. W. (1993) *Anal. Biochem.* **209,** 32–44
21. Sreerema, N., Venyaminov, S. Y., and Woody, R. W. (1999) *Protein Sci.* **8,** 370–380
22. Provencher, S. W., and Glockner, J. (1981) *Biochemistry* **20,** 33–37
23. Johnson, W. C. (1999) *Proteins* **35,** 307–312
24. Santambrogio, P., Levi, S., Arosio, P., Palagi, L., Vecchio, G., Lawson, D. M., Yewdall, S. J., Artymiuk, P. J., Harrison, P. M., Jappelli, R., and Cesareni, G. (1992) *J. Biol. Chem.* **267,** 14077–14083
25. Santambrogio, P., Levi, S., Cozzi, A., Rovida, E., Albertini, A., and Arosio, P. (1993) *J. Biol. Chem.* **268,** 12744–12748
26. Scatchard, G. (1949) *Ann. N. Y. Acad. Sci.* **51,** 660–672
27. Saneto, R. P., and De Vellis, J. (1987) *Neurochemistry: A Practical Approach* (Turner, H. J., and Bachelard, H. S., eds) pp. 27–63, IRL Press, Washington, D.C.
28. Cassina, P., Peluffo, H., Pehar, M., Martinez-Palma, L., Ressia, A., Beckman, J. S., Estevez, A. G., and Barbeito, L. (2002) *J. Neurosci. Res.* **67,** 21–29
29. Vidal, R., Miravalle, L., Gao, X., Barbeito, A. G., Baraibar, M. A., Hekmatyar, S. K., Widel, M., Bansal, N., Delisle, M. B., and Ghetti, B. (2008) *J. Neurosci.* **28,** 60–67
30. Martsev, S. P., Vlasov, A. P., and Arosio, P. (1998) *Protein Eng.* **11,** 377–381
31. Kim, S., Kim, Y., and Lee, J. (2001) *Biochem. Biophys. Res. Commun.* **289,** 125–129
32. Stefanini, S., Cavallo, S., Wang, C. Q., Tataseo, P., Vecchini, P., Giartosio, A., and Chiancone, E. (1996) *Arch. Biochem. Biophys.* **325,** 58–64
33. Fontana, A., Zambonin, M., Polverino de Laureto, P., De Filippis, V., Clementi, A., and Scaramella, E. (1997) *J. Mol. Biol.* **266,** 223–230
34. Fontana, A., Fassina, G., Vita, C., Dalzoppo, D., Zamai, M., and Zambonin, M. (1986) *Biochemistry* **25,** 1847–1851
35. Wolz, R., and Bond, J. (1990) *Anal. Biochem.* **191,** 314–320
36. Santambrogio, P., Cozzi, A., Levi, S., Rovida, E., Magni, F., Albertini, A., and Arosio, P. (2000) *Protein Expression Purif.* **19,** 212–218
37. Cuff, J. A., and Barton, G. J. (1999) *Proteins* **40,** 502–511
38. Chou, P. Y., and Fasman, G. D. (1978) *Adv. Enzymol. Relat. Areas Mol. Biol.* **47,** 45–148
39. Granier, T., Gallois, B., Langlois d'Estaintot, B., Dautant, A., Chevalier, J. M., Mellado, J. M., Beaumont, C., Santambrogio, P., Arosio, P., and Precigoux, G. (2001) *Acta Crystallogr. Sect. D Biol. Crystallogr.* **57,** 1491–1497
40. Levi, S., Luzzago, A., Franceschinelli, F., Santambrogio, P., Cesareni, G., and Arosio, P. (1989) *Biochem. J.* **264,** 381–388
41. Bou-Abdallah, F., Arosio, P., Santambrogio, P., Yang, X., Janus-Chandler, C., and Chasteen, N. (2002) *Biochemistry* **41,** 11184–11191
42. Luzzago, A., and Cesareni, G. (1989) *EMBO J.* **8,** 569–576
43. Jappelli, R., Luzzago, A., Tataseo, P., Pernice, I., and Cesareni, G. (1992) *J. Mol. Biol.* **227,** 532–543
44. Jappelli, R., and Cesareni, G. (1998) *Biochem. Biophys. Res. Commun.* **250,** 342–346
45. Ingrassia, R., Gerardi, G., Biasiotto, G., and Arosio, P. (2006) *J. Biochem.* (*Tokyo*) **139,** 881–885
46. Cozzi, A., Santambrogio, P., Corsi, B., Campanella, A., Arosio, P., and Levi, S. (2006) *Neurobiol. Dis.* **23,** 644–652
47. Yang, D., Matsubara, K., Yamaki, M., Ebina, S., and Nagayama, K. (1994) *Biochim. Biophys. Acta* **1206,** 173–179